THE JOURNAL OF PHYSICAL CHEMISTRY A

Article

pubs.acs.org/JPCA

Near-Edge X-ray Absorption Fine Structure Spectra and Site-Selective Dissociation of Phenol

Yi-Shiue Lin,[†] Kun-Ta Lu,[†] Yuan T. Lee,[‡] Chien-Ming Tseng,[§] Chi-Kung Ni,[‡,∥] and Chen-Lin Liu*[,†]

[†]Scientific Research Division, National Synchrotron Radiation Research Center, Hsinchu 30076, Taiwan

[‡]Institute of Atomic and Molecular Sciences, Academia Sinica, Taipei 10617, Taiwan

[§]Department of Applied Chemistry, National Chiao Tung University, Hsinchu 30010, Taiwan

[∥]Department of Chemistry, National Tsing Hua University, Hsinchu 30013, Taiwan

ABSTRACT: A time-of-flight mass spectrometer with orthogonal acceleration and soft X-rays from synchrotron radiation were utilized to measure near-edge X-ray absorption fine structure (NEXAFS) spectra of carbon and oxygen in phenol and the corresponding ionic fragments following core excitation. The photon energies were in the range of 284−298 eV for the carbon K-edge and 529.5−554.5 eV for the oxygen K-edge. The total ion yield, ion intensity for each ionic fragment, and ion intensity ratio, defined as ion intensity divided by total ion yield, were measured as a function of photon energy. Possible mechanisms of dissociation are proposed and enhancements of specific products of dissociation are reported. In general, the enhancement of these specific products is small in the carbon K-edge region but is clear for some products at the oxygen K-edge. In particular, elimination of the H atom from the hydroxyl group was observed only at the oxygen K-edge. One remarkable result is that an excitation of a core-level electron of oxygen greatly enhanced the cleavage of specific C−C bonds.

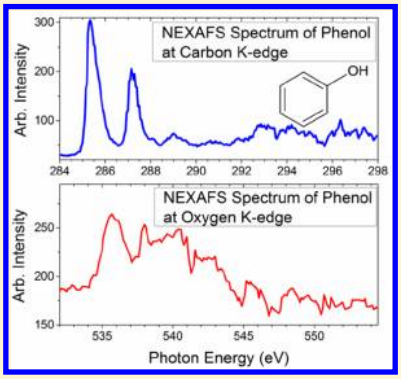

INTRODUCTION

In the early 1920s the wavelengths of X-ray absorption edges were discovered to depend on the chemical environment of atoms of a particular element.[1,2] Near-edge X-ray absorption fine structure (NEXAFS) spectra soon proved to provide a sensitive technique to determine accurately the electronic structure of matter and for chemical analysis.[3−8] The range of shifts of soft X-ray absorption spectra for a given element due to varied chemical environments is from a few hundred millielectronvolts to several electronvolts. For instance, the C 1s → $\pi^*_{C=O}$ excitation for a carbonate is blue-shifted as much as 4 eV relative to that of an aldehyde.[9]

When molecules are irradiated with X-rays, one core electron is excited to a valence orbital or directly ionized, forming a hole in the inner shell of the atom. The excited molecules then undergo Auger decay or photon emission. Auger decay is the major channel because fluorescence yields for carbon and oxygen atoms are typically small (0.2575% and 0.6909%, respectively).[10] After emission of one or two electrons following Auger decay, the resulting molecular ions are mostly unstable and dissociate into charged and neutral fragments. Eberhardt and co-workers first observed a site-specific fragmentation upon core excitation.[11,12] Selective bond breaking on excitation of inner-shell electrons of a chosen atom has received increasing attention,[13−16] in part due to the availability of a third-generation synchrotron light source.[17−22]

Site-selective fragmentation using core−electron excitation has been observed for several molecules in gaseous samples as well as on surfaces.[23−31] Two instances of site-specific dissociation of a gaseous sample are CF_3CH_3 and CF_2CH_2 reported by Klaus and co-workers;[32] ions containing fluorine atoms (CF_3^+, $C_2F_2H_2^+$, and CF_2^+) are dominant products when the core of carbon connected to hydrogen atoms is excited. These observed phenomena demonstrate that chemical bonds near the excited atom have a greater probability of cleavage. Poly(methyl methacrylate) (PMMA) is an example of site-specific dissociation on a surface. When a core electron of oxygen is excited to $\sigma^*(O-CH_3)$, cleavage of the $O-CH_3$ bond is enhanced, but the $C-OCH_3$ bond is more likely to break when the core electron is excited to $\sigma^*(C-OCH_3)$.[21]

Site-specific fragmentation of aromatic molecules has been found for 2-amino-3-methylpyridine,[33] 2-fluoropyridine,[34] and pyrimidine derivatives[35−38] following excitation of electrons from C 1s and N 1s orbitals. The dissociation of phenol is of great interest[39−43] because phenol is the chromophore of amino acid tyrosine. Excitation of an electron from the O 1s orbital or C 1s orbital of a carbon atom attached to an oxygen atom in phenol is expected to show site-specific dissociation. In this work, we investigated NEXAFS spectra of carbon and oxygen in gaseous phenol and the dissociation channels following core excitation, focusing attention on ionic products from site-specific or bond-specific dissociation.

EXPERIMENTS

A new reflectron time-of-flight mass spectrometer with orthogonal acceleration (OA-R-TOF MS) was constructed in

Received: January 10, 2014
Revised: February 7, 2014
Published: February 7, 2014

   dx.doi.org/10.1021/jp500284r | J. Phys. Chem. A 2014, 118, 1601−1609

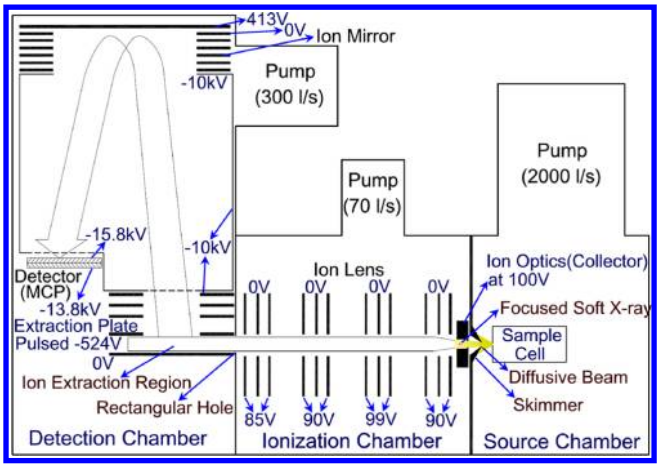

Figure 1. Schematic diagram of the apparatus. For clarity of depiction, this figure is not drawn to scale according to real instruments. An effusive molecular beam was generated in the source chamber. Molecules were ionized in the ionization chamber. Ions were accelerated by the electric field of the ion optics (collector) then collimated with the ion lens in the ionization chamber. Masses were analyzed with a reflectron time-of-flight mass spectrometer with orthogonal acceleration in the detection chamber. The soft X-rays crossed the effusive molecular beam in the ionization chamber. The direction of propagation of the soft X-rays was perpendicular to the effusive molecular beam and perpendicular to the plane of the figure.

Taiwan Light Source, National Synchrotron Radiation Research Center. Figure 1 shows a schematic diagram of this apparatus that includes a source chamber, an ionization chamber, and a detection chamber. A diffusive molecular beam of phenol was generated in the source chamber from a sample cell with an orifice of diameter 0.15 mm. The sample cell was kept at 308 K; the pressure of phenol inside the cell was estimated to be 0.8 Torr. The diffused molecular beam was collimated with a skimmer (2 mm diameter) located 8 mm downstream from the sample cell before it entered the ionization chamber. The skimmer separated the source chamber from ionization chamber and kept the pressure of ionization chamber low. During the experiment the pressures in the source chamber and ionization chamber were 2.7×10^{-6} and 1×10^{-6} Torr, respectively.

Soft X-rays from synchrotron radiation were directed into the ionization chamber with a pair of bendable refocusing Kirkpatrick–Baez mirrors coated with Au and were focused at the effusive molecular beam. The propagation direction of the soft X-rays was perpendicular to the effusive molecular beam. Soft X-rays crossed the diffusive molecular beam 20 mm downstream from the skimmer. The crossing point of the soft X-rays and effusive molecular beam was located inside an ion optics (collector). Molecules ionized with X-ray photons dissociated into ionic fragments when a large internal energy was left in the cations. Ions (parent ions or ionic fragments) generated with soft X-rays were accelerated by the electric field of the ion optics (collector) and pushed into the ion lens region; collimated with the ion lenses, they flew through a rectangular hole that separated the ionization chamber and detection chamber before entering the ion-acceleration region of a reflectron time-of-flight mass spectrometer with orthogonal acceleration in the detection chamber.[44−47] The rectangular hole (8.8 ×40 mm^2) was designed so that most collimated ions would pass through it, but it also kept the pressure in the detection chamber about one tenth that in the ionization chamber. During the experiment the pressure in the detection chamber was 4.3×10^{-8} Torr. Voltages applied on the ion optic (collector) and ion lenses were adjusted to optimize the mass resolution. Ion trajectories simulated with SIMION (version 8.1 by Scientific Instrument Services) showed that ions with kinetic energy less than 3 eV can be 100% collected and sent to the detection chamber. The collection efficiency decreased as the ion kinetic energy increased for ions with kinetic energy greater than 3 eV. Ions with kinetic energy greater than 3 eV and velocity nearly perpendicular to the axis of the ion lens were not collected.

When ions flew into the ion-acceleration region, a pulsed voltage was applied on the extraction plate and ions were accelerated along the axis perpendicular to their initial direction of motion. The repetition rate of the pulsed voltage was 50 kHz. Each voltage pulse generated a mass spectrum. The results were the accumulation of 1×10^6 mass spectra in each step (50 meV/step) at the carbon K-edge and 4×10^6 mass spectra in each step (150 meV/step) at the oxygen K-edge. All ions were accelerated to 15.8 keV before they reached the detector. Ions were detected with a chevron-configured microchannel-plate (MCP) detector (95 × 42 mm^2). The large kinetic energy of ions ensured that the discrimination between various ions was minimized. Xe ions generated from X-rays, of which m/z ranged from 21 to 134 u for various Xe isotope ions with charges 1−6, served for mass calibration.

The output signal from the MCP was amplified with a preamplifier and recorded with a rapid time-of-flight multiscaler (FAST ComTec, model P7888) with 2 ns bin width. The probability of two ions of the same m/z arriving the detector at the same time was small (10^{-6}) because of the small X-ray photon flux. A counting technique was utilized to accumulate the signal; a discrimination level was set to obtain an optimal signal-to-noise ratio.

As details of the synchrotron radiation beamline have been reported,[48] only a brief description is provided here. This beamline delivers >10^{12} photons/s with energy in the 60−1400 eV range. Energy resolution ($E/\Delta E$) might be as great as 20,000, depending on the widths of open slits and the grating. In this experiment, energy resolutions were about 150 meV at the carbon K-edge region and 250 meV at the oxygen K-edge region. The size of the beam spot was 0.4 mm ×0.2 mm at the intersection with the diffusive molecular beam. The photon energy was calibrated with absorption spectra of CO_2 for both the carbon K-edge (290.77 eV) and the oxygen K-edge (535.4 eV).[31,49−54]

Phenol (Sigma Aldrich, 99%) was purified with three freeze−pump−thaw cycles to remove the impurities in the sample cell.

RESULTS

Carbon K-edge. The total ion yield (TIY) of phenol NEXAFS spectra at the carbon K-edge from 284 to 298 eV is shown in Figure 2. To assign the spectra, we compared the reported spectra of benzene,[55−59] aniline,[56,60] and phenol.[9,56,61] Duflot and co-workers analyzed a high-resolution NEXAFS spectrum of benzene utilizing electron energy loss.[55,62−66] The first intense absorption of benzene at 285.2 eV is assigned as the transition 1s → π^*. A small absorption at 287.24 eV is attributed to the transition 1s → 3sσ in which the latter MO is composed mostly of $a_1(C_e{-}H)^*$. The major feature at 289.09 eV is assigned to arise from an excitation to Rydberg states. The following lines (290.6 and 293.8 eV) are assigned as excitation of a core electron to σ^*, Rydberg states, or a mixture of both;

dx.doi.org/10.1021/jp500284r | J. Phys. Chem. A 2014, 118, 1601−1609

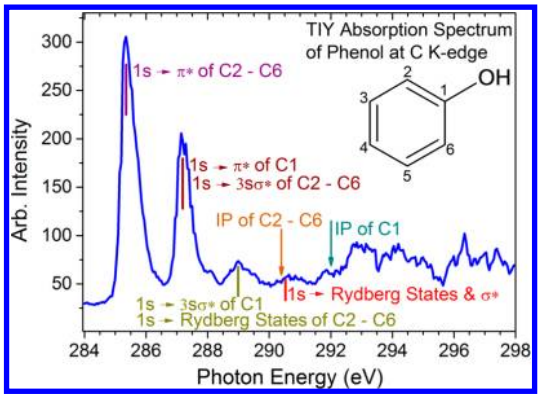

Figure 2. NEXAFS spectrum of phenol excited from 284 to 298 eV in a total ion yield mode. The scanning step was 50 meV, and the photon-energy resolution was 150 meV. The numbers of carbon atoms as well as the suggested assignments are exhibited. The ionization potentials of carbon atoms are also represented.

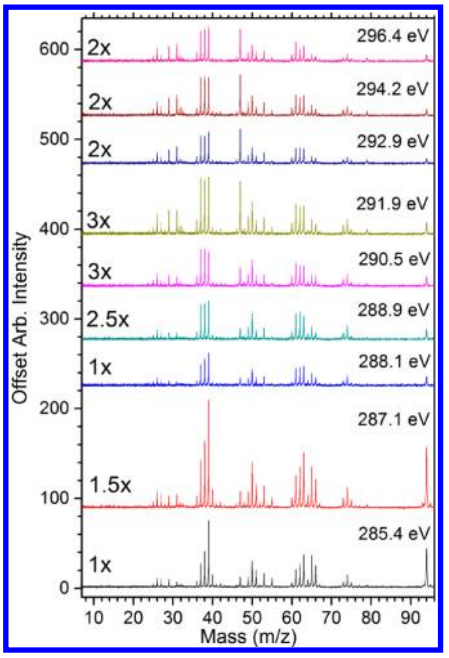

Figure 3. Mass spectra of the dissociation of phenol following core excitation and Auger decay. These excitation energies were chosen according to the narrow or broad lines in the carbon NEXAFS spectrum of phenol (Figure 2). For a sufficient signal-to-noise ratio, the integrating times vary, as noted at each mass spectrum.

the core ionization threshold was found to be 290.3 eV.[55,62−69] When one hydrogen atom of benzene was replaced by an amino group or a hydroxyl group, the absorption signal of the carbon atom beside the nitrogen or oxygen atom was blue-shifted by 1.5 or 1.8 eV, respectively.[56] On comparison with the spectra of benzene, aniline, and phenol previously investigated, the two major absorption lines of phenol centered at 285.4 and 287.1 eV were assigned as 1s → π^* of C2−C6 and a mixture of 1s → π^* of C1 and 1s → 3sσ^* of C2−C6, respectively. Cn (n = 1 − 6) denotes the position of carbon atoms in phenol, as shown in Figure 2. The broad line at 288.9 eV is assigned as a mixture of an excitation to Rydberg states from a core electron of C2−C6 and 1s → 3sσ^* of C1. Another weak broad line centered at 290.5 eV is composed of transitions from a core level to Rydberg states and σ^* orbitals. Beyond 290.4 and 292 eV, C2−C6 and C1, respectively,[56] were directly ionized. These assignments are listed in table 1.

Figure 3 shows the mass spectra of product ions from phenol excited at various photon energies at the absorption signals in our NEXAFS spectrum. The major product ions are similar, although the relative intensities vary with the photon energy. Of the ion intensities as a function of photon energy for several major product ions in Figure 4, most show large intensities at 285.4 and 287.1 eV attributed to the resonant excitation shown as the lines in the NEXAFS spectrum at these two energies. A small signal centered at 288.9 eV in Figure 2 can also be observed for some ions.

To reveal the phenomena of specific dissociation following core excitation, the ion intensity ratios, defined as ion intensity for each ion in Figure 4 divided by the total ion intensity in Figure 2, are shown in Figure 5 for major product ions. In the following paragraphs, we propose possible compositions of ions and mechanisms of dissociation.

Two lines located at 285.4 and 287.1 eV, observed for parent ion (with m/z = 94 u), represent a large probability of no cracking and no second ejection of an electron after ionization.

Table 1. Assignments of Absorption Lines and Ionization Energies of Core Excitation[a]

Carbon K-edge	
experimental value	assignment
285.4 eV	1s → π^* of C2−C6
287.1 eV	1s → π^* of C1 and 1s → 3sσ^* of C2−C6
288.9 eV	1s → 3sσ^* of C1 and 1s → Rydberg states of C2−C6
290.5 eV	1s → Rydberg states and σ^*
290.4 eV	IP of C2−C6[56]
292 eV	IP of C1[56]
Oxygen K-edge	
experimental value	assignment
535.52 eV	1s → σ^*[67] and 1s → π^* with contribution of 1s → σ^*_{O-H}[61]
537.98 eV	1s → π^*[61,67] and 1s → Rydberg states[4]
540 eV	1s → σ^* or Rydberg states[4,61,67] and 1s → continuum range beyond IP[4,61,67]
538.90 eV	IP[67]

[a]The locations of the lines were the positions of maximum absorption. The uncertainty due to energy resolution of the light source, overlap of some transitions, and initial and final vibrational states were estimated to be slightly greater than the energy resolution of the light source (150 meV for the carbon K-edge and 250 meV for the oxygen K-edge).

dx.doi.org/10.1021/jp500284r | J. Phys. Chem. A 2014, 118, 1601−1609

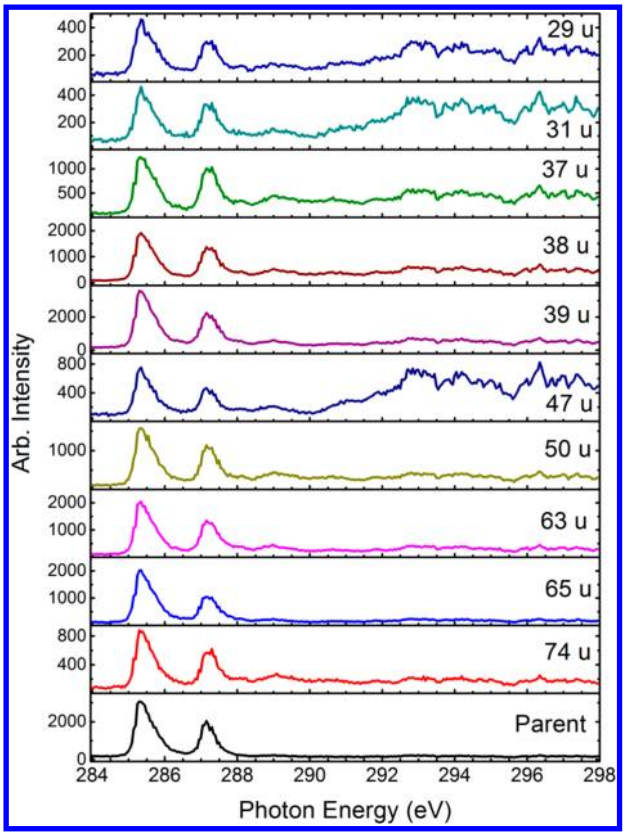

Figure 4. Intensities of major product ions produced after exciting a core electron of phenol in carbon atoms varying with photon energy. These curves are similar to the NEXAFS spectrum coupled with some subtle differences detailed in the text.

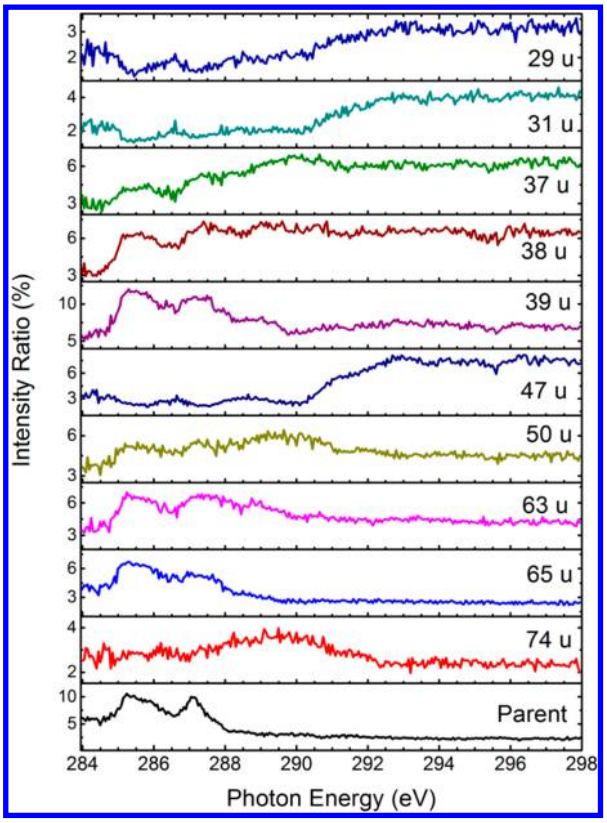

Figure 5. Intensity ratios of major product ions produced after exciting a core electron of phenol in its carbon atoms. These ratios are obtained from the curves of intensity variation (Figure 4) divided by the TIY NEXAFS spectrum (Figure 2). In this figure, the fractions of each ionic product at varied photon energy reveal some enhancements of dissociation channels following specific excitations.

The intensity of the second line is slightly smaller than that of the first line. The first line represents excitation 1s → π^* of C2−C6, followed by ejection of an Auger electron that takes away most energy. The energy left for some phenol cations is so small that their dissociation does not occur, resulting in parent ions. The second line represents an excitation of a mixture of 1s → π^* of C1 and 1s → 3sσ^* of C2−C6. For the excitation to a π^* unoccupied orbital, an Auger electron might also remove most energy, resulting in the production of parent ions. Molecules excited to a σ^* orbital might, in contrast, dissociate rapidly into fragments because of the antibonding character of the σ^* orbital. As a result, the intensity of the second line in Figure 5, at 287.1 eV, is smaller than the intensity of the first line, at 285.4 eV. The intensity of the parent ion becomes small when the photon energy exceeds the core ionization threshold because most ions either become doubly charged cations and appear at m/z = 47 u or dissociate into two cations.

An ion with m/z = 47 u represents the doubly charged parent ion ($C_6H_5OH^{2+}$) that is the only possible composition. The ion intensity ratio, illustrated in Figure 5, shows that the generation of doubly charged parent ions is greatly enhanced for a photon energy greater than the core ionization threshold (290.4 eV). This observation is rationalized from the fact that direct core ionization followed by ejection of an Auger electron (normal Auger decay) can readily generate doubly charged ions. The presence of such doubly charged parent ions indicates that some Auger electron takes away most energy such that some doubly charged ions are stabilized. Although spectator or participant Auger decay was the dominant process for photon energy less than the ionization energy (290.4 eV) whereby singly charged parent ions were typically formed, we observed doubly charged parent ions (with m/z = 47 u) also for photon energy less than the ionization energy, 290.4 eV, likely because of autoionization following Auger decay.

A fragment ion with m/z = 77 u ($C_6H_5^+$) resulted from cleavage of the C−O bond through OH elimination, and fragment ions with m/z = 72 − 76 u represented elimination of additional H atoms following cleavage of that C−O bond. The possible compositions are listed in Table 2. A possible dissociation channel is shown in Figure 6a. Among these fragments, enhancement phenomena were observed only for those with m/z = 74 and 75 u ($C_6H_2^+$ and $C_6H_3^+$); the signal of $C_6H_2^+$ had the largest intensity. Although it is expected that the excitation of a C1 core electron at 287.1 eV has a larger probability to break the C−O bond, no enhancement of this fragment ion was observed in this region. A small broad line centered about 289.5 eV was observed, but no line with a large intensity ratio was found for this fragment in Figure 5. The broad line is near the excitations C2−C6 C1s → Rydberg states, C1 C1s → 3sσ^*, and another transition to σ^* orbitals, but no clear site-specific dissociation is assignable.

Fragment ions with m/z = 60 (C_5^+), 61 (C_5H^+), 62 ($C_5H_2^+$), and 63 u ($C_5H_3^+$) resulting from the elimination of COH with additional H atoms require the cleavage of both C−C bonds connecting carbon atom C1 shown as in Figure 6b. The excitation of a C1 core electron at 287.1 eV is expected to have a larger probability to generate these fragments when a site-

dx.doi.org/10.1021/jp500284r | J. Phys. Chem. A 2014, 118, 1601−1609

Table 2. Formula of Major Ionic Products and Possible Bond Cleavages

m/z (u)	molecular formula	possible bond cleavage	*m/z* (u)	molecular formula	possible bond cleavage
26	$C_2H_2^+$	Figure 6c1,c2	60	C_5^+	Figure 6b
27	$C_2H_3^+$	Figure 6c1,c2	61	C_5H^+	Figure 6b
28	CO^+ or $C_2H_4^+$	Figure 6b or Figure 6c1,c2	62	$C_5H_2^+$	Figure 6b
29	CHO^+ or $C_2H_5^+$	Figure 6b or Figure 6c1,c2	63	$C_5H_3^+$	Figure 6b
31	CH_3O^+	unknown	64	$C_5H_4^+$	Figure 6b
36	C_3^+	Figure 6e	65	C_4HO^+ or $C_5H_5^+$	Figure 6c1,c2 or Figure 6b
37	C_3H^+	Figure 6e	66	$C_4H_2O^+$ or $C_5H_6^+$	Figure 6c1,c2 or unknown
38	$C_3H_2^+$	Figure 6e	72	C_6^+	Figure 6a
39	$C_3H_3^+$	Figure 6e	73	C_6H^+	Figure 6a
47	$C_6H_5OH^{2+}$	none	74	$C_6H_2^+$	Figure 6a
49	C_4H^+	Figure 6d	75	$C_6H_3^+$	Figure 6a
50	$C_4H_2^+$	Figure 6d	76	$C_6H_4^+$	Figure 6a
51	$C_4H_3^+$	Figure 6d	77	$C_6H_5^+$	Figure 6a
53	C_3HO^+	Figure 6e	79	$C_5H_3O^+$	losing CH and two hydrogen atoms
54	$C_3H_2O^+$	Figure 6e	93	$C_6H_5O^+$	losing one hydrogen atom
55	$C_3H_3O^+$	Figure 6e	94	$C_6H_5OH^+$	none

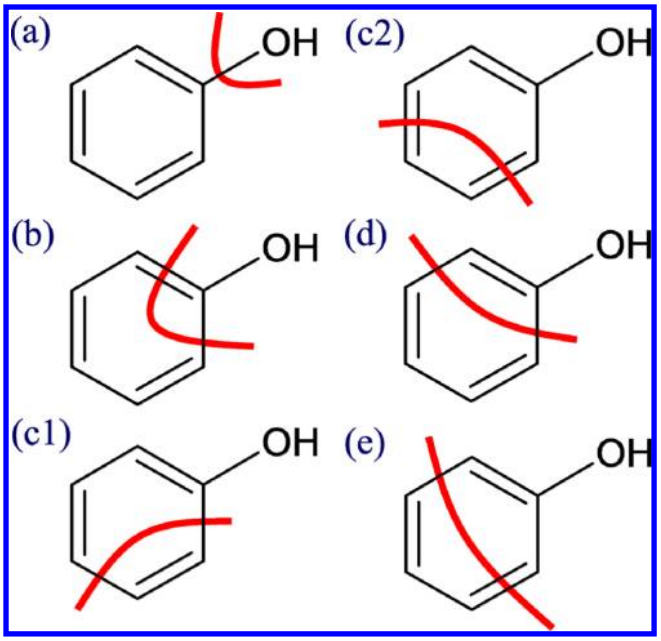

Figure 6. Schematic diagrams of possible paths of dissociation and the corresponding broken chemical bonds. Some products were formed with some H atoms elimination following these paths. Panels c1 and c2 are both for C_2H_2 elimination, but separate chemical bonds are broken.

specific dissociation occurs, but the enhancements are not limited to this photon energy. The enhancements were observed at 285.5, 287.6, and 289 eV for m/z = 63 u ($C_5H_3^+$). For those involving loss of more hydrogen atoms (m/z = 62, 61, and 60 u), the enhancements were not clear, but a broadened small enhancement centered at 290 eV was observed. The other fragment of this dissociation channel is COH, which might exhibit the same intensity and intensity ratio if the positive charge were equally located at each side of the fragment. The intensity ratio of the COH^+ ion differs markedly, however, from that for m/z = 60−63 u, as shown in Figure 4 and 5.

Fragment ions with m/z = 66 ($C_4H_2O^+$ or $C_5H_6^+$) and 65 u (C_4HO^+ or $C_5H_5^+$) can result from the elimination of C_2H_2 with an elimination of additional H atoms or from elimination of CO and COH, respectively. The corresponding possible bond cleavages involving loss of C_2H_2 are shown in Figure 6c1,c2. The elimination of C_2H_2 can include the cleavage of chemical bonds connected to C1 or exclude the cleavage of chemical bonds connecting to C1. Elimination of CO from a phenol cation has a small barrier;[70] it was also observed in electron-impact ionization.[71] Again, CO elimination requires the cleavage of both C−C bonds connected to C1. The feature of ion intensity ratios at m/z = 65 and 66 u are similar: enhancement was not limited to the corresponding excitation (287.1 eV) but existed at both 285.4 and 287.1 eV. One possible explanation is that these fragment ions include at least C_2H_2 elimination.

The dominant products are $C_3H_3^+$ (with m/z = 39 u) and related fragments (C_3^+, C_3H^+, and $C_3H_2^+$ with m/z = 36−38 u). To generate cation $C_3H_3^+$, cleavage of two C−C bonds is necessary; these bonds might be C1−C2 and C4−C5, or C2−C3 and C5−C6, as in Figure 6e. The former includes a chemical bond connecting atom C1, but the latter is unrelated to atom C1; as a result, enhancement is expected at both 285.4 and 287.1 eV. The enhancement is large for $C_3H_3^+$ at both 285.4 and 287.1 eV. The enhancement was small for $C_3H_2^+$ and zero for C_3^+ and C_3H^+. Almost no enhancement was observed for the other fragment of this channel, i.e., $C_3H_3O^+$ (with m/z = 55 u), indicating that the positive charge is not located equally on each side during dissociation.

For the other fragments, both the ion intensity and the enhancement from bond-specific dissociation are small; we accordingly omit discussion thereof.

Oxygen K-edge. The total ion yield mode of the NEXFAS spectrum is shown in Figure 7. This spectrum comprises two lines at 535.52 and 537.98 eV and a broad line centered about 540 eV. The line at 535.52 eV was assigned as 1s → σ^* of which the molecular orbital is significantly composed of a carbon 2p orbital.[67] Although Francis and Hitchcock assigned this line as exciting to π^*, there is also a contribution of 1s → σ^*_{O-H}.[61] Prince and co-workers compared the spectra and theoretical calculation of tautomers of guanine; the structures of the two tautomers are similar to that of phenol. They assigned the first line to a transition between a core electron in oxygen and Rydberg states (3s orbital) coupled with an unoccupied π^* molecular orbital.[4] The line at 537.98 eV was assigned as 1s → π^*[61,67] or as excitation to Rydberg states.[4] The broad line centered at 540 eV marks the transition to σ^* or Rydberg states as well as a continuum range beyond the ionization energy.[4,61,67] Some small lines appeared about 545 eV, but no assignment was reported.[61,67] The assignments and ionization energy of oxygen atom are listed in table 1.

Shown in Figure 8 are mass spectra of phenol excited at specific energies; these mass spectra are similar to those from the carbon K-edge excitation. One interesting difference is that fragment ion $C_6H_5O^+$ (m/z = 93 u), corresponding to elimination of one H atom, was clearly observed only from excitation at the oxygen K-edge. Strong intensity of a fragment ion was observed also before the photon energy reached that of excitation of the oxygen core electron. This result is attributed

dx.doi.org/10.1021/jp500284r | J. Phys. Chem. A 2014, 118, 1601−1609

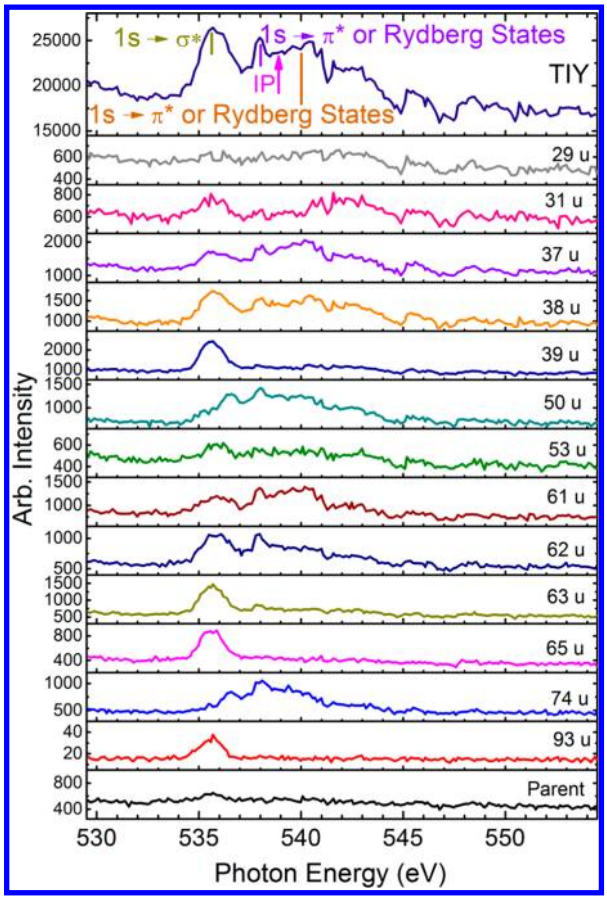

Figure 7. NEXAFS spectrum of phenol in the total ion-yield mode excited from 529.5 to 554.5 eV and intensity variations of major ionic products. Each scanning step is 150 meV; the photon energy resolution is 250 meV. In the NEXAFS spectrum, the assignments are represented and the ionization energy of the oxygen atom is indicated with a vertical arrow.

to an absorption tail of a core electron of a carbon atom, but the absorption cross section is about one tenth that at 290 eV.

Intensities and intensity ratios as a function of photon energy of major product ions are shown in Figure 7 and 9, respectively. Bond-specific dissociations observed from the ion intensity ratio in this region of photon energy are classified into three groups: one with enhancement at 535.5 eV, including ions with m/z = 93 ($C_6H_5O^+$), 65 (C_4HO^+ or $C_5H_5^+$), 63 ($C_5H_3^+$), and 39 u ($C_3H_3^+$), another with enhancement about the broad line from 536 to 541 eV, including m/z = 74 ($C_6H_2^+$), 61 (C_5H^+), and 50 u ($C_4H_2^+$), and a third group with enhancement at both lines exhibited by ions m/z = 62 ($C_5H_2^+$) and 38 u ($C_3H_2^+$).

If a site-specific dissociation of a bond occurs on excitation of an oxygen core electron, fragments corresponding to cleavage of O−H and C−O bonds are expected to have large ion-intensity ratios (Figure 9). Fragments related to these bond cleavages are ions $C_6H_5O^+$ (m/z = 93 u, O−H bond cleavage) and $C_6H_2^+$ (m/z = 74 u, cleavage of C−O and a subsequent elimination of additional H atoms). Enhancements were found for these two fragment ions: $C_6H_5O^+$ ions have a large enhancement at 535.5 eV and were clearly observed only from excitation at the oxygen K-edge. $C_6H_2^+$ ions have enhancement from 537 to 545 eV. Although the other fragment ions have also a significantly enhanced ratio of ion intensities, for example, ions $C_3H_3^+$, $C_5H_3^+$, C_4HO^+, and $C_5H_5^+$ at photon energy 535.5 eV, the mechanism of ion generation of these

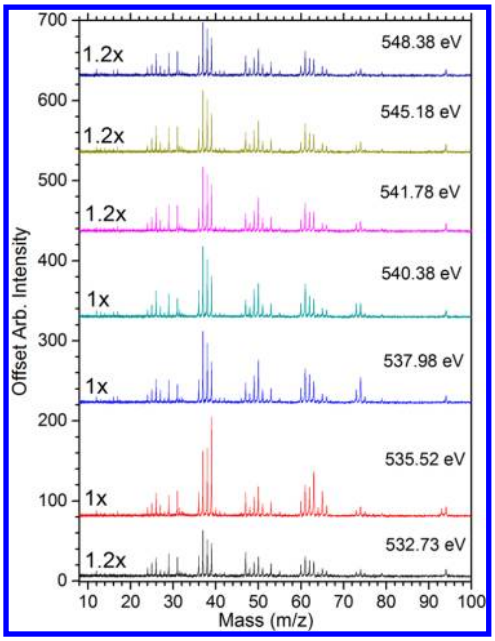

Figure 8. Mass spectra of dissociation of phenol following core excitation and Auger decay at the oxygen K-edge. These excitation energies are selected for narrow lines, broad lines, and before the main absorption region in the oxygen NEXAFS spectrum of phenol (top of Figure 7). The integration periods for various excitation energies vary as noted with each mass spectrum.

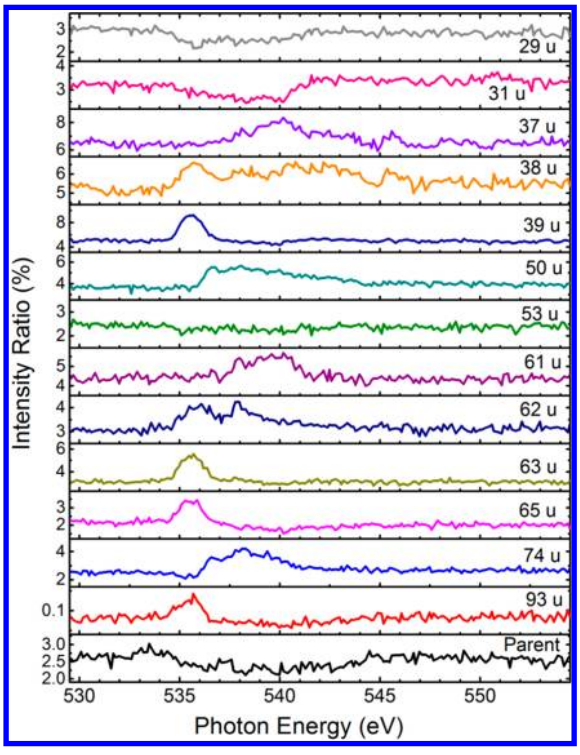

Figure 9. Intensity ratios of major ionic products produced after excitation of a core electron of phenol in the oxygen atom. These ratios are obtained from the curves of intensity variation (Figure 7) divided by the TIY NEXAFS spectrum (top panel of Figure 7). In this figure the fraction of each ionic product at various photon energies is represented. The narrow and broad lines reveal the enhancements of some dissociation paths following specific excitations detailed in the text.

dx.doi.org/10.1021/jp500284r | J. Phys. Chem. A 2014, 118, 1601−1609

fragments excludes the chemical bond directly connecting the O atom.

DISCUSSION

Specific dissociations are generally separated into two types: element-specific and site-specific. This classification is attributed to the excitation of separate elements and varied chemical environments of the same elements, respectively.[18] A possible mechanism leading to a specific dissociation is the localization of excitation and rapid dissociation following a core excitation and an Auger decay. If the final state after Auger decay is localized at one specific atom or chemical bond and the rate of dissociation is greater than that of energy redistribution, dissociation is more likely to occur around this excited atom. One example is the excitation to a σ^* orbital of a specific chemical bond. If this electron stays in this antibonding orbital even after Auger decay, the antibonding characteristic results in rapid dissociation along this chemical bond. In contrast, if the redistribution of the intramolecular energy is more rapid than dissociation, excess energy is distributed to all degrees of freedom, which results in dissociation according to statistical predictions. The branching ratios among various dissociation channels are hence expected to vary slowly with the photon energy.

A major absorption line of phenol centered at 287.1 eV is assigned as a mixture of transitions 1s → π^* of C1 and 1s → 3sσ^* of C2−C6. The transition 1s → 3sσ^* of C2−C6 can greatly enhance the cleavage of a chemical bond connecting carbon atoms C2−C6. We observed only a small enhancement of the ion intensity ratio at this photon energy for ions with m/z = 39 ($C_3H_3^+$), 50 ($C_4H_2^+$), 63 ($C_5H_3^+$, elimination of COH with additional H atoms elimination), and 65 u ($C_5H_5^+$, elimination of COH). The generation of these ions is related to the cleavage of a chemical bond connecting carbon atoms C2−C6. The broad line at 288.9 eV is assigned as a mixture of an excitation to Rydberg states from a core electron of C2−C6 and C1 1s → 3sσ^*. The transition 1s → 3sσ^* of C1 favors the cleavage of a chemical bond connecting C1. The cleavages of specific bonds at this photon energy involve fission of the C1−O bond generating an ionic fragment $C_6H_2^+$ (m/z = 74 u) and fission of the C1−C2 bond resulting in an ion $C_4H_2^+$ (m/z = 50 u). This enhancement is also small, but large enhancements were found for ions $C_3H_2^+$, $C_3H_3^+$, $C_5H_3^+$, C_4HO^+, and $C_5H_5^+$ at 285.4 eV (assigned as 1s → π^* of C2−C6). The generations of these fragments are related to the cleavage of chemical bonds connecting carbon atoms C2−C6. Although no antibonding orbitals are involved directly in the core excitation, a large enhancement of the ion ratio at this photon energy indicates that the energy left after an Auger decay is localized around the initially excited atoms.

The spectrum at the oxygen K-edge comprises two lines at 535.52 and 537.98 eV and one broad line centered about 540 eV. The signal at 535.52 eV is assigned as 1s → σ^*. Enhancements of the ion intensity at this photon energy were found for $C_6H_5O^+$ (H atom elimination), C_4HO^+ or $C_5H_5^+$ (m/z = 65 u), $C_5H_3^+$, $C_3H_3^+$, and $C_3H_2^+$. Only the fragment $C_6H_5O^+$ is related to the cleavage of a chemical bond connecting the O atom. The line at 537.98 eV is assigned as 1s → π^*[61,67] or excitation to Rydberg states.[4] The enhancement of the ion intensity at this photon energy involved ions $C_6H_2^+$, C_5H^+, and $C_4H_2^+$. Only fragment $C_6H_2^+$ (elimination of OH and additional elimination of three H atoms) is related to the chemical bond connecting the O atom.

Specific dissociation was defined also as the ion intensity difference between core excitation and ionization with electron impact at energy 70 eV.[18,72] The major fragment ions of phenol obtained from such ionization include the parent ion and those with m/z = 39, 40, 65, and 66 u. Ions with m/z = 26, 27, 29, 37, 38, 47, 50, 51, 53, 55, 61−64, 67, and 74 u have small intensities.[71] Compared to our result, many product ions (CHO^+, $C_2H_5^+$, CH_3O^+, $C_6H_5OH^{2+}$, $C_4H_2^+$, $C_4H_3^+$, C_5H^+, $C_5H_2^+$, $C_5H_3^+$, $C_6H_2^+$, and $C_6H_5O^+$) are enhanced through specific dissociation at both carbon and oxygen K-edges. In particular, an elimination of a H atom from the phenol cation ($C_6H_5O^+$ with m/z = 93 u) was not observed from ionization with electron impact, but was observed following a core excitation of oxygen, which indicates that a core excitation of oxygen can specifically break the O−H bond.

Nguyen and co-workers[70] measured the mass spectrum of ionized phenol following collisional activation (8 keV) in a nitrogen cell. The main product ions (with m/z = 26, 29, 39, 50, 55, 63, 65, 74 u) are similar to those from core excitation, although the corresponding intensities differ. The mass spectrum with the greatest abundance of an ionic product with m/z = 65 u and the next greatest abundance of an ion product with m/z = 39 u was found from collisional activation, indicating a distinct mechanism of ionization and dissociation.

The energy levels of ionized phenol and its isomers and the reaction mechanism of loss of CO have been explored with quantum chemical calculations.[70] In the path with least energy, the elimination of CO begins from the migration of the hydrogen atom on the hydroxyl group to the β carbon (C2), followed by ring-opening, closure of a five-membered ring, and elimination of CO. In this mechanism of least energy, the energies of all transition species are less than that of the first step, hydrogen migration. CO elimination that has a small energy barrier is the major dissociation channel for phenol cations with small internal energy.

It is likely that energy greater than 10 eV was left in the phenol cation after excitation of a core electron to unoccupied orbitals and Auger decay. A similar large energy left in a cation was found in pyrimidine.[37] Many electronic excited states might be involved during the dissociation because of a large energy left in a cation. The dissociation products also indicate that the dissociation paths must be complicated. The identification of the detailed dissociation paths with the current experimental and theoretical methods is difficult and is beyond the scope of this work.

AUTHOR INFORMATION

Corresponding Author

*Phone: +886-3-5780281, ext 7337. Fax: +886-3-5783813. E-mail: Liu.CL@nsrrc.org.tw.

Notes

The authors declare no competing financial interest.

ACKNOWLEDGMENTS

National Science Council (NSC), Taiwan, supported this work under Contract NSC 100-2113-M-213-004-MY2. We thank Prof. Wei-Ping Hu for many helpful discussions in assignments of NEXAFS spectra.

REFERENCES

(1) Lindh, A. Zur Kenntnis des Röntgenabsorptionsspektrums von Chlor. *Z. Phys.* **1921**, *6*, 303−310.

(2) Siegbahn, M. *Spektroskopie der Röntgenstrahlen*; Berlin: Springer Verlag, 1931.
(3) Vall-llosera, G.; Gao, B.; Kivimaki, A.; Coreno, M.; Ruiz, J. A.; Simone, M. d.; Agren, H.; Rachlew, E. The C 1s and N 1s Near Edge X-ray Absorption Fine Structure Spectra of Five Azabenzenes in the Gas Phase. *J. Chem. Phys.* **2008**, *128*, 044316.
(4) Plekan, O.; Feyer, V.; Richter, R.; Coreno, M.; Vall-llosera, G.; Prince, K. C.; Trofimov, A. B.; Zaytseva, I. L.; Moskovskaya, T. E.; Gromov, E. V.; et al. An Experimental and Theoretical Core-Level Study of Tautomerism in Guanine. *J. Phys. Chem. A* **2009**, *113*, 9376−9385.
(5) Feyer, V.; Plekan, O.; Richter, R.; Coreno, M.; de Simone, M.; Prince, K. C.; Trofimov, A. B.; Zaytseva, I. L.; Schirmer, J. Tautomerism in Cytosine and Uracil: A Theoretical and Experimental X-ray Absorption and Resonant Auger Study. *J. Phys. Chem. A* **2010**, *114*, 10270−10276.
(6) Graf, N.; Yegen, E.; Gross, T.; Lippitz, A.; Weigel, W.; Krakert, S.; Terfort, A.; Unger, W. E. S. XPS and NEXAFS Studies of Aliphatic and Aromatic Amine Species on Functionalized Surfaces. *Surf. Sci.* **2009**, *603*, 2849−2860.
(7) Oji, H.; Mitsumoto, R.; Ito, E.; Ishii, H.; Ouchi, Y.; Seki, K.; Yokoyama, T.; Ohta, T.; Kosugi, N. Core Hole Effect in NEXAFS Spectroscopy of Polycyclic Aromatic Hydrocarbons: Benzene, Chrysene, Perylene, and Coronene. *J. Chem. Phys.* **1998**, *109*, 10409−10418.
(8) Samuel, N. T.; Lee, C.-Y.; Gamble, L. J.; Fischer, D. A.; Castner, D. G. NEXAFS Characterization of DNA Components and Molecular-Orientation of Surface-Bound DNA Oligomers. *J. Electron Spectrosc. Relat. Phenom.* **2006**, *152*, 134−142.
(9) Cooney, R. R.; Urquhart, S. G. Chemical Trends in the Near-Edge X-ray Absorption Fine Structure of Monosubstituted and Para-Bisubstituted Benzenes. *J. Phys. Chem. B* **2004**, *108*, 18185−18191.
(10) Hubbell, J. H.; Trehan, P. N.; Singh, N.; Chand, B.; Mehta, D.; Garg, M. L.; Garg, R. R.; Singh, S.; Puri, S. A Review, Bibliography, and Tabulation of K, L, and Higher Atomic Shell X-Ray Fluorescence Yields. *J. Phys. Chem. Ref. Data* **1994**, *23*, 339−364.
(11) Eberhardt, W.; Sham, T. K.; Carr, R.; Krummacher, S.; Strongin, M.; Weng, S. L.; Wesner, D. Site-Specific Fragmentation of Small Molecules Following Soft-X-Ray Excitation. *Phys. Rev. Lett.* **1983**, *50*, 1038−1041.
(12) Eberhardt, W.; Stöhr, J.; Feldhaus, J.; Plummer, E. W.; Sette, F. Correlation between Electron Emission and Fragmentation into Ions following Soft-X-Ray Excitation of the N_2 Molecule. *Phys. Rev. Lett.* **1983**, *51*, 2370−2373.
(13) Lago, A. F.; Cavasso-Filho, R. L.; de Souza, G. G. B.; Santos, A. C. F.; Stolte, W. C.; Schlachter, A. S. Anionic and Cationic Photodissociation of the Chloroform Molecule Excited in the Vicinity of the Cl 1s Edge. *Chem. Phys. Lett.* **2012**, *543*, 34−40.
(14) Stolte, W. C.; Ohrwall, G.; Sant'Anna, M. M.; Lopez, I. D.; Dang, L. T. N.; Piancastelli, M. N.; Lindle, D. W. 100% Site-Selective Fragmentation in Core-Hole-Photoexcited Methanol by Anion-Yield Spectroscopy. *J. Phys. B: At., Mol. Opt. Phys.* **2002**, *35*, L253−L259.
(15) Eland, J. H. D.; Linusson, P.; Mucke, M.; Feifel, R. Homonuclear Site-Specific Photochemistry by an Ion-Electron Multi-Coincidence Spectroscopy Technique. *Chem. Phys. Lett.* **2012**, *548*, 90−94.
(16) Lu, K. T.; Chen, J. M.; Lee, J. M.; Chen, C. K.; Chou, T. L.; Chen, H. C. State-Specific Dissociation Enhancement of Ionic and Excited Neutral Photofragments of Gaseous CCl_4 and Solid-State Analogs Following Cl 2p Core-Level Excitation. *New J. Phys.* **2008**, *10*, 053009.
(17) Chen, J. M.; Lu, K. T.; Lee, J. M.; Ma, C. I.; Lee, Y. Y. State Selective Enhanced Production of Excited Fragments and Ionic Fragments of Gaseous $Si(CH_3)_2Cl_2$ and Solid-State Analogs following Core-Level Excitation. *Phys. Rev. Lett.* **2004**, *92*, 243002.
(18) Baba, Y. Element-Specific and Site-Specific Ion Desorption from Adsorbed Molecules by Deep Core-Level Photoexcitation at the K-Edges. *Low Temp. Phys.* **2003**, *29*, 228−242.
(19) Bernini, R. B.; da Silva, L. B. G.; Rodrigues, F. N.; Coutinho, L. H.; Rocha, A. B.; de Souza, G. G. B. Core Level (S 2p) Excitation and Fragmentation of the Dimethyl Sulfide and Dimethyldisulfide Molecules. *J. Chem. Phys.* **2012**, 136.
(20) Wada, S.-i.; Sumii, R.; Isari, K.; Waki, S.; Sako, E. O.; Sekiguchi, T.; Sekitani, T.; Tanaka, K. Active Control of Chemical Bond Scission by Site-Specific Core Excitation. *Surf. Sci.* **2003**, *528*, 242−248.
(21) Wada, S.-i.; Kizaki, H.; Matsumoto, Y.; Sumii, R.; Tanaka, K. Selective Chemical Bond Breaking Characteristically Induced by Resonant Core Excitation of Ester Compounds on a Surface. *J. Phys.: Condens. Matter* **2006**, *18*, S1629−S1653.
(22) Gerones, M.; Erben, M. F.; Romano, R. M.; Cavasso Filho, R. L.; Della Vedova, C. O. Interstellar H_3^+ and HCS^+ Ions Produced in the Dissociative Photoionization Process of $CH_3C(O)SCH_3$ in the Proximity of the Sulfur 2p, Carbon 1s, and Oxygen 1s Edges. *J. Phys. Chem. A* **2012**, *116*, 2571−2582.
(23) Schmelz, H. C.; Reynaud, C.; Simon, M.; Nenner, I. Site-Selective Fragmentation in Core-Excited Bromo-Chloro-Alkanes $[Br(CH_2)_nCl]$. *J. Chem. Phys.* **1994**, *101*, 3742−3749.
(24) Nenner, I.; Reynaud, C.; Schmelz, H. C.; Ferrand-Tanaka, L.; Simon, M.; Morin, P. Site Selective Fragmentation with Soft X-rays: From Gaseous Polyatomic Molecules, Free Clusters, Polymers, Adsorbates to Biological Macromolecules. *Z. Phys. Chem.* **1996**, *195*, 43−63.
(25) Miron, C.; Simon, M.; Leclercq, N.; Hansen, D. L.; Morin, P. Site-Selective Photochemistry of Core Excited Molecules: Role of the Internal Energy. *Phys. Rev. Lett.* **1998**, *81*, 4104−4107.
(26) Naves de Brito, A.; Sundin, S.; Marinho, R. R.; Hjelte, I.; Fraguas, G.; Gejo, T.; Kosugi, N.; Sorensen, S. L.; Björneholm, O. Memories of Excited Femtoseconds: Effects of Core−Hole Localization after Auger Decay in the Fragmentation of Ozone. *Chem. Phys. Lett.* **2000**, *328*, 177−187.
(27) Kukk, E.; Rius i Riu, J.; Tankiewicz, M.; Hatherly, P. A.; Erman, P.; Rachlew, E.; Winiarczyk, P.; Huttula, M.; Aksela, S. Dissociation of Deuteromethane Following Carbon 1s Core Ionization. *Phys. Rev. A* **2002**, *66*, 012704.
(28) Liu, X. J.; Prümper, G.; Kukk, E.; Sankari, R.; Hoshino, M.; Makochekanwa, C.; Kitajima, M.; Tanaka, H.; Yoshida, H.; Tamenori, Y.; et al. Site-Selective Ion Production of the Core-Excited CH_3F Molecule Probed by Auger-Electron−Ion Coincidence Measurements. *Phys. Rev. A* **2005**, *72*, 042704.
(29) Prümper, G.; Ueda, K.; Hergenhahn, U.; De Fanis, A.; Tamenori, Y.; Kitajima, M.; Hoshino, M.; Tanaka, H. 3D-Ion-Momentum/High-Resolution-Electron Coincidence Measurements. *J. Electron Spectrosc. Relat. Phenom.* **2005**, *144*−*147*, 227−230.
(30) Kobayashi, E.; Mase, K.; Nambu, A.; Seo, J.; Tanaka, S.; Kakiuchi, T.; Okudaira, K. K.; Nagaoka, S.-i.; Tanaka, M. Recent Progress in Coincidence Studies on Ion Desorption Induced by Core Excitation. *J. Phys.: Condens. Matter* **2006**, *18*, S1389−S1408.
(31) Sodhi, R. N. S.; Brion, C. E. Reference Energies for Inner Shell Electron Energy-Loss Spectroscopy. *J. Electron Spectrosc. Relat. Phenom.* **1984**, *34*, 363−372.
(32) Habenicht, W.; Baiter, H.; Mueller-Dethlefs, K.; Schlag, E. W. Memory Effects in Molecular Fragmentation Induced by Site-Specific Core Excitation Using a Reflection Time-of-Flight Mass Spectrometer. *J. Phys. Chem.* **1991**, *95*, 6774−6780.
(33) Okada, K.; Sakai, M.; Ohno, K. Specific Fragmentation of K-Shell Excited/Ionized Pyridine Derivatives Studied by Electron Impact: 2-Amino-3-methylpyridine and 3-Methylpyridine. *Bull. Chem. Soc. Jpn.* **2008**, *81*, 1580−1583.
(34) Sakai, M.; Okada, K. Effect of Fluoro Substitution on the Fragmentation of the K-Shell Excited/Ionized Pyridine Studied by Electron Impact. *J. Mass Spectrom.* **2011**, *46*, 666−671.
(35) Ptasińska, S.; Denifl, S.; Grill, V.; Märk, T. D.; Illenberger, E.; Scheier, P. Bond- and Site-Selective Loss of H- from Pyrimidine Bases. *Phys. Rev. Lett.* **2005**, *95*, 093201.
(36) Itala, E.; Ha, D. T.; Kooser, K.; Nommiste, E.; Joost, U.; Kukk, E. Fragmentation Patterns of Core Ionized Uracil. *Int. J. Mass Spectrom.* **2011**, *306*, 82−90.

(37) Bolognesi, P.; O'Keeffe, P.; Feyer, V.; Plekan, O.; Prince, K.; Coreno, M.; Mattioli, G.; Bonapasta, A. A.; Zhang, W.; Carravetta, V.; et al. Inner Shell Excitation, Ionization and Fragmentation of Pyrimidine. *J. Phys.: Conf. Ser.* **2010**, *212*, 012002.
(38) Itala, E.; Ha, D. T.; Kooser, K.; Huels, M. A.; Rachlew, E.; Nommiste, E.; Joost, U.; Kukk, E. Molecular Fragmentation of Pyrimidine Derivatives Following Site-Selective Carbon Core Ionization. *J. Electron Spectrosc. Relat. Phenom.* **2011**, *184*, 119−124.
(39) Tseng, C.-M.; Lee, Y. T.; Lin, M.-F.; Ni, C.-K.; Liu, S.-Y.; Lee, Y.-P.; Xu, Z. F.; Lin, M. C. Photodissociation Dynamics of Phenol. *J. Phys. Chem. A* **2007**, *111*, 9463−9470.
(40) Bussandri, A.; van Willigen, H. FT-EPR Study of the Wavelength Dependence of the Photochemistry of Phenols. *J. Phys. Chem. A* **2002**, *106*, 1524−1532.
(41) Hermann, R.; Mahalaxmi, G. R.; Jochum, T.; Naumov, S.; Brede, O. Balance of the Deactivation Channels of the First Excited Singlet State of Phenols: Effect of Alkyl Substitution, Sterical Hindrance, and Solvent Polarity. *J. Phys. Chem. A* **2002**, *106*, 2379−2389.
(42) Tseng, C.-M.; Lee, Y. T.; Ni, C.-K. H Atom Elimination from the $\pi\sigma^*$ State in the Photodissociation of Phenol. *J. Chem. Phys.* **2004**, *121*, 2459−2461.
(43) Nix, M. G. D.; Devine, A. L.; Cronin, B.; Dixon, R. N.; Ashfold, M. N. R. High Resolution Photofragment Translational Spectroscopy Studies of the Near Ultraviolet Photolysis of Phenol. *J. Chem. Phys.* **2006**, *125*, 133318.
(44) Guilhaus, M.; Selby, D.; Mlynski, V. Orthogonal Acceleration Time-of-Flight Mass Spectrometry. *Mass Spectrom. Rev.* **2000**, *29*, 65−107.
(45) Coles, J.; Guilhaus, M. Orthogonal Acceleration—A New Direction for Time-of-Flight Mass Spectrometry: Fast, Sensitive Mass Analysis for Continuous Ion Sources. *TrAC, Trends Anal. Chem.* **1993**, *12*, 203−213.
(46) Dawson, J. H. J.; Guilhaus, M. Orthogonal-Acceleration Time-of-Flight Mass Spectrometer. *Rapid Commun. Mass Spectrom.* **1989**, *3*, 155−159.
(47) Selby, D. S.; Mlynski, V.; Guilhaus, M. A 20 kV Orthogonal Acceleration Time-of-Flight Mass Spectrometer for Matrix-Assisted Laser Desorption/Ionization. *Int. J. Mass Spectrom.* **2001**, *210−211*, 89−100.
(48) Chung, S. C.; Chen, J.; Huang, L. R.; Wu, R. T.; Chen, C. C.; Cheng, N. F.; Chuang, J. M.; Tseng, P. C.; Huang, D. J.; Chang, C. F.; et al. Performance of an Elliptically Polarized Undulator Beamline. *Nucl. Instrum. Methods Phys. Res., Sect. A* **2001**, *467−468* (Part 1), 445−448.
(49) Sham, T. K.; Yang, B. X.; Kirz, J.; Tse, J. S. K-Edge Near-Edge X-ray-Absorption Fine Structure of Oxygen- and Carbon-Containing Molecules in the Gas Phase. *Phys. Rev. A* **1989**, *40*, 652−659.
(50) Vall-llosera, G.; Huels, M. A.; Coreno, M.; Kivimäki, A.; Jakubowska, K.; Stankiewicz, M.; Rachlew, E. Photofragmentation of 2-Deoxy-D-Ribose Molecules in the Gas Phase. *ChemPhysChem* **2008**, *9*, 1020−1029.
(51) Tronc, M.; King, G. C.; Read, F. H. Carbon K-Shell Excitation in Small Molecules by High-Resolution Electron Impact. *J. Phys. B: At. Mol. Phys.* **1979**, *12*, 137−157.
(52) Tronc, M.; King, G. C.; Read, F. H. Nitrogen K-Shell Excitation in N_2, NO and N_2O by High-Resolution Electron Energy-Loss Spectroscopy. *J. Phys. B: At., Mol. Opt. Phys.* **1980**, *13*, 999−1008.
(53) Wight, G. R.; Brion, C. E. K-Shell Energy Loss Spectra of 2.5 keV Electrons in CO_2 and N_2O. *J. Electron Spectrosc. Relat. Phenom.* **1974**, *3*, 191−205.
(54) Feyer, V.; Plekan, O.; Richter, R.; Coreno, M.; Prince, K. C.; Carravetta, V. Core Level Study of Alanine and Threonine. *J. Phys. Chem. A* **2008**, *112*, 7806−7815.
(55) Duflot, D.; Flament, J. P.; Heinesch, J.; Hubin-Franskin, M. J. Re-Analysis of the K-Shell Spectrum of Benzene. *J. Electron Spectrosc. Relat. Phenom.* **2000**, *113*, 79−90.
(56) Solomon, J. L.; Madix, R. J.; Stöhr, J. Orientation and Absolute Coverage of Benzene, Aniline, and Phenol on Ag(110) Determined by NEXAFS and XPS. *Surf. Sci.* **1991**, *255*, 12−30.
(57) Bradeanu, I. L.; Flesch, R.; Kosugi, N.; Pavlychev, A. A.; Ruhl, E. C 1s → π^* Excitation in Variable Size Benzene Clusters. *Phys. Chem. Chem. Phys.* **2006**, *8*, 1906−1913.
(58) Flesch, R.; Serdaroglu, E.; Blobner, F.; Feulner, P.; Brykalova, X. O.; Pavlychev, A. A.; Kosugi, N.; Ruhl, E. Gas-to-Solid Shift of C 1s-Excited Benzene. *Phys. Chem. Chem. Phys.* **2012**, *14*, 9397−9402.
(59) Menzel, D.; Rocker, G.; Steinruck, H. P.; Coulman, D.; Heimann, P. A.; Huber, W.; Zebisch, P.; Lloyd, D. R. Core Excitation, Decay, and Fragmentation in Solid Benzene as Studied by X-Ray Absorption, Resonant Auger, and Photon Stimulated Desorption. *J. Chem. Phys.* **1992**, *96*, 1724−1734.
(60) Huang, S. X.; Fischer, D. A.; Gland, J. L. Correlation between the Surface Configurations and Hydrogenolysis: Aniline on the Pt(111) Surface. *J. Vac. Sci. Technol., A* **1994**, *12*, 2164−2169.
(61) Francis, J. T.; Hitchcock, A. P. Inner-Shell Spectroscopy of *p*-Benzoquinone, Hydroquinone, and Phenol: Distinguishing Quinoid and Benzenoid Structures. *J. Phys. Chem.* **1992**, *96*, 6598−6610.
(62) Eberhardt, W.; Haelbich, R. P.; Iwan, M.; Koch, E. E.; Kunz, C. Fine Structure at the Carbon 1s K-edge in Vapours of Simple Hydrocarbons. *Chem. Phys. Lett.* **1976**, *40*, 180−184.
(63) Hitchcock, A. P.; Brion, C. E. Carbon K-Shell Excitation of C_2H_2, C_2H_4, C_2H_6 and C_6H_6 by 2.5 keV Electron Impact. *J. Electron Spectrosc. Relat. Phenom.* **1977**, *10*, 317−330.
(64) Horsley, J. A.; Stohr, J.; Hitchcock, A. P.; Newbury, D. C.; Johnson, A. L.; Sette, F. Resonances in the K Shell Excitation Spectra of Benzene and Pyridine: Gas Phase, Solid, and Chemisorbed States. *J. Chem. Phys.* **1985**, *83*, 6099−6107.
(65) Medhurst, L. J.; Ferrett, T. A.; Heimann, P. A.; Lindle, D. W.; Liu, S. H.; Shirley, D. A. Observation of Correlation Effects in Zero Kinetic Energy Electron Spectra near the N1s and C1s Thresholds in N_2, CO, C_6H_6, and C_2H_4. *J. Chem. Phys.* **1988**, *89*, 6096−6102.
(66) Hitchcock, A. P.; Fischer, P.; Gedanken, A.; Robin, M. B. Antibonding σ^* Valence MOs in the Inner-Shell and Outer-Shell Spectra of the Fluorobenzenes. *J. Phys. Chem.* **1987**, *91*, 531−540.
(67) Plashkevych, O.; Yang, L.; Vahtras, O.; Ågren, H.; Petterson, L. G. M. Substituted Benzenes as Building Blocks in near-Edge X-ray Absorption Spectra. *Chem. Phys.* **1997**, *222*, 125−137.
(68) Jolly, W. L.; Bomben, K. D.; Eyermann, C. J. Core-Electron Binding Energies for Gaseous Atoms and Molecules. *At. Data Nucl. Data Tables* **1984**, *31*, 433−493.
(69) Hu, C.-H.; Chong, D. P. Density Functional Computations for Inner-Shell Excitation Spectroscopy. *Chem. Phys. Lett.* **1996**, *262*, 729−732.
(70) Le, H. T.; Flammang, R.; Gerbaux, P.; Bouchoux, G.; Nguyen, M. T. Ionized Phenol and Its Isomers in the Gas Phase. *J. Phys. Chem. A* **2001**, *105*, 11582−11592.
(71) NIST Chemistry WebBook: NIST Standard Reference Database Number 69. http://webbook.nist.gov. Linstrom, P.J., Mallard, W.G., Eds.; NIST Mass Spec Data Center.
(72) Sekiguchi, T.; Ikeura-Sekiguchi, H.; Baba, Y. Site-Specific Fragmentation of Acetone Adsorbates on Si(100) in the Carbon 1s Absorption Edge. *Surf. Sci.* **2000**, *454−456*, 363−368.